


Article

Volume Estimation of Landslide Affected Soil Moisture Using TRIGRS: A Case Study of Longxi River Small Watershed in Wenchuan Earthquake Zone, China

Tong Sun, Zhiyuan Deng, Zexing Xu and Xiekang Wang * 

State Key Laboratory of Hydraulics and Mountain River Engineering, Sichuan University, Chengdu 610065, China; suntong9711@163.com (T.S.); dengzhiyuan2019@163.com (Z.D.); zexingxu@163.com (Z.X.)

* Correspondence: wangxiekang@scu.edu.cn

Abstract: After the 2008 M_w 7.9 Wenchuan earthquake, geological hazards occurred frequently in the southwest mountainous watershed. Frequent landslide disasters provide abundant sediment supply for mountain torrent disasters. The estimation of the potential landslide volume is essential for the risk assessment of mountain torrent disasters. In this study, a method of calculation that combines TRIGRS and the slope-units for estimating the landslide volume of a small mountainous watershed has been established. TRIGRS analyzes the watershed landslide safety factor under rainfall conditions based on grid-cells. The slope-units extract the results and combine the empirical power law formula to calculate the potential landslide volume. In this paper, we use this method to assess the landslide volume of the Longxi river basin. The results show that the area and volume estimates of the landslides are consistent with the results observed from satellite images and field surveys. This method can be used to study the impact of sediment transport on mountain torrent disasters in the basin. With different moisture content conditions, the results show that the soil moisture content and slope angle significantly affect the distribution and volume of potential landslides in the watershed, giving rise to the uncertainty of the landslide estimation.



Citation: Sun, T.; Deng, Z.; Xu, Z.; Wang, X. Volume Estimation of Landslide Affected Soil Moisture Using TRIGRS: A Case Study of Longxi River Small Watershed in Wenchuan Earthquake Zone, China. *Water* **2021**, *13*, 71. <https://doi.org/10.3390/w13010071>

Received: 16 November 2020

Accepted: 28 December 2020

Published: 31 December 2020

Publisher's Note: MDPI stays neutral with regard to jurisdictional claims in published maps and institutional affiliations.



Copyright: © 2020 by the authors. Licensee MDPI, Basel, Switzerland. This article is an open access article distributed under the terms and conditions of the Creative Commons Attribution (CC BY) license (<https://creativecommons.org/licenses/by/4.0/>).

Keywords: mountain river; slope-units; landslide volume; soil moisture

1. Introduction

In China, mountain torrents is a very common natural disaster with wide distribution, high frequency, strong regionality, and strong seasonality [1,2]. It is particularly severe in the southwestern mountainous area and southeast coastal hilly area from May to September. In the southwestern area of China, it has huge terrain undulations and complex geological structures. Especially after the “5.12” Wenchuan earthquake in 2008, a large number of collapses and landslides occurred. The secondary geological disasters in Wenchuan have been obviously aggravated, providing sufficient source supplements for mountain torrents and debris flows [3]. Wang et al. pointed out that about 60,000 landslides occurred in the Wenchuan earthquake disaster area [4]. Parker et al. proposed that the volume of loose sources produced by collapses, landslides, and mudslides in the Wenchuan earthquake disaster area reached 5–15 km³ [5]. Tang et al. pointed out that the main reason for the Wenjiagou disaster is that a large number of loose deposits were generated after the Wenchuan earthquake [6]. Large numbers of loose deposits flow into the river channel, causing the river channel to be blocked and raising the river bed. The mountainous watershed of Sichuan often has short-term heavy rainfall, resulting in the characteristics of strong destructiveness, short duration, and strong suddenness of flash flood disasters. The landslide area after an earthquake provides an abundant source supplement for mountain flood disaster [7]. Landslides have a major impact on the hydrological response of local areas [8]. Moreover, the corresponding early warning system is not complete, and the relative lack of data brings difficulties to the debris flow early warning [2]. A

significant amount of sediment transport in a flash flood disaster have been contributed by the landslide volume of the landslides. Evaluation of the volume of the potentially landslide on the slope is vital for hazard mitigation.

When conducting landslide disaster assessment, the physics-based model combined with hydrogeological models is often used to evaluate the stability of the area, such as SHALSTAB (shallow landslide stability model) [9–11] based on the infinite slope considering the steady seepage of rainfall, TRIGRS (transient rainfall infiltration and grid-based regional slope-stability model) [12,13] based on the change of pore water pressure caused by transient infiltration and the three-dimensional deterministic model Scoops3D developed by the US Bureau of Quality Investigation.

TRIGRS model has been widely used in the world. Tang et al. used TRIGRS and the point-estimate method to effectively simulate the landslide scenarios in Badong County [14]. Roberto et al. used TRIGRS model to estimating rainfall intensity and duration thresholds in a tropical mountainous basin of the Valle de Aburrá [15]. Chen et al. estimated the landslide in Dehua County by coupling GRAPES model and TRIGRS model [16].

When evaluating geological disasters, the estimation method of landslide volume has been continuously improved with the innovation of remote sensing and GIS. With the improvement of high-resolution digital terrain data, the volume of loose materials can be analyzed by the pre- and post-event DEMs [17,18]. In the estimation of the landslide area and volume, the potential area can be obtained by satellite images. Chang et al. interpreted satellite images in different periods in the Longxi River. The statistical results showed that the landslide area changed with time [19]. Tang et al. used high-resolution aerial photography and satellite images to extract a set of landslide deposit volumes [20]. Chiu et al. further estimated the potential volume of landslides based on the analytic hierarchy process (AHP) and the landslide volume is estimated by the empirical power law formula [21]. The relationship was exponential, established by the scale index γ , and intercept α . The relationship is as follows:

$$V = \alpha A^\gamma \quad (1)$$

Many scholars have applied this formula based on different landslides. Guzzetti et al. selected 677 global single landslide cases and derived the empirical relationship between landslide volume and landslide area [22]. Larson et al. has made a statistical analysis of 4231 groups of shallow and deep landslides and obtained the reference range of corresponding parameter values [23]. Parker et al. revised the α and γ for the Wenchuan earthquake region based on field measurements [5].

In the process of geological hazard assessment, grid-cells, terrain units, slope-units, unique-condition units, and topographical units are often used for watershed treatment [24]. Grid-cells and slope-units are often used in regional stability analysis [25]. Slope-units are divided by river valley lines and mountain ridge lines. Yan et al. proposed an improved method of slope-units division based on the basin division principle of curvature of Romstad et al. [26,27]. Alvioli et al. propose an extraction method to ensure slope homogeneity based on the definition of maximum homogeneity of slope element [28,29]. Wang et al. proposed an extraction method based on MIA-HSU through morphological image analysis [25,30].

In this study, we selected the Longxi river small watershed, which is prone to geological disasters for study. We obtained the change of soil moisture content in a year through the field investigation of a local flash flood gully. The corresponding soil mechanical parameters were selected based on the investigation results. TRIGRS is used to simulate and evaluate landslide risk based on grid-cells. Then, the landslide risk coefficient is extracted by slope-units to obtain the local landslide area. Finally, the volume is estimated by using the empirical power law formula of area volume. The estimation results are compared with the interpretation of satellite images and post-disaster field survey results.

2. Methods

2.1. TRIGRS Model

TRIGRS (the transient rainfall infiltration and grid-based regional slope-stability model) is a FORTRAN program used to calculate the spatio-temporal variation of safety factor distribution caused by a rainfall [31]. The model solves the complex rainfall process and an impermeable basal boundary at finite depth and a simple runoff routing scheme. The model is extended by using the analytical solution of the Richards equation of vertical permeation to address infiltration into a partially unsaturated layer above the water [12,13,32]. This model treats the soil as a two-layer system, including a saturated zone with a capillary fringe above the water table, covered with an unsaturated zone extending to the ground [13] (Figure 1).

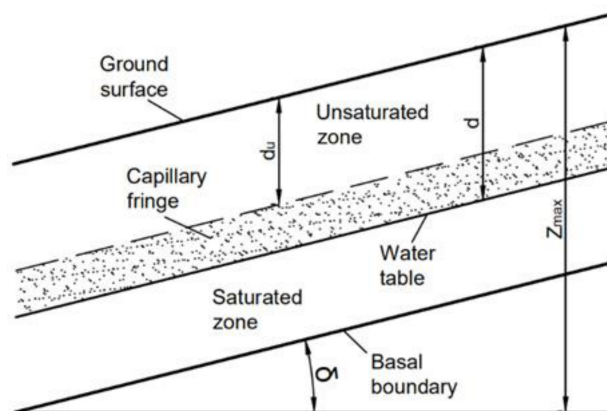


Figure 1. Conceptual diagram of the TRIGRS model [13].

The model uses a series of Heaviside step functions to solve the proposed sum of the original solutions for constant intensity rainfall proposed by Iversobbbbn to represent a general time-varying sequence of surface fluxes of different intensity and duration [33]. The generalized solution used in TRIGRS is as follows:

$$\begin{aligned} \psi(Z, t) = & (Z - d)\beta \\ & + 2 \sum_{n=1}^N \frac{I_{nZ}}{K_s} H(t - t_n) [D_1(t - t_n)]^{\frac{1}{2}} \sum_{m=1}^{\infty} \left\{ \text{ierfc} \left[\frac{(2m-1)d_{LZ} - (d_{LZ} - Z)}{2[D_1(t - t_n)]^{\frac{1}{2}}} \right] + \text{ierfc} \left[\frac{(2m-1)d_{LZ} + (d_{LZ} - Z)}{2[D_1(t - t_n)]^{\frac{1}{2}}} \right] \right\} \\ & - 2 \sum_{n=1}^N \frac{I_{nZ}}{K_s} H(t - t_{n+1}) [D_1(t - t_{n+1})]^{\frac{1}{2}} \sum_{m=1}^{\infty} \left\{ \text{ierfc} \left[\frac{(2m-1)d_{LZ} - (d_{LZ} - Z)}{2[D_1(t - t_{n+1})]^{\frac{1}{2}}} \right] + \text{ierfc} \left[\frac{(2m-1)d_{LZ} + (d_{LZ} - Z)}{2[D_1(t - t_{n+1})]^{\frac{1}{2}}} \right] \right\} \end{aligned} \quad (2)$$

where ψ is the groundwater pressure head, t is the time, Z is the soil thickness, d is the depth of the water table, K is the saturated hydraulic vertical conductivity, I_{nZ} is the surface flux at time n , N is the total number of time intervals, $D_1 = D_0 / \cos^2 \delta$, D_0 is the saturated hydraulic permeability coefficient, δ is the slope angle, d_{LZ} is the boundary of the impervious base, and m is a coefficient showing an infinite series of odd terms.

ierfc is the complementary error function [13], which is defined as the following equation:

$$\text{ierfc}(\eta) = \frac{1}{\sqrt{\pi}} \exp(-\eta^2) - \eta \text{erfc}(\eta) \quad (3)$$

The connection of several parameters in the Richard equation for the soil characteristic curve of unsaturated soil is obtained by the Garden exponential hydraulic parameter model [34]. The expression is as follows:

$$K(\psi) = K_s \exp(\alpha \psi^*) \quad (4)$$

$$\theta = \theta_r + (\theta_s - \theta_r) \exp(\alpha \psi^*) \quad (5)$$

where ψ is the pressure head, $K(\psi)$ is the hydraulic conduction function, the pressure head at the top of the capillary edge, $\psi^* = \psi - \psi_0$, α is obtained by fitting the soil characteristic curve parameter.

2.2. Calculation Method

We first collected relevant parameters of the watershed through field investigation and literature review, including DEM, hydraulic parameters, soil parameters, and rainfall data. Slope-units of the watershed are made according to the curvature. These parameters are input into the TRIGRS model to calculate the risk coefficient map of the basin [26,27]. Slope-units are defined by watersheds in the mean-curvature image. The production steps of this method can be implemented in GIS. Secondly, the obtained coefficient graph is segmented by slope-units. The average of the safety factors on all grid cells within each slope cell is the value of all grid cells within that slope cell. When the safety factor is less than 1, the unit is considered a dangerous unit (Figure 2). Finally, the area of each dangerous slope unit is sorted out, and the landslide volume of each dangerous slope unit is obtained through the formula. The total landslide volume in the basin is obtained by adding the landslide volumes of all dangerous slope-units (Figure 3).

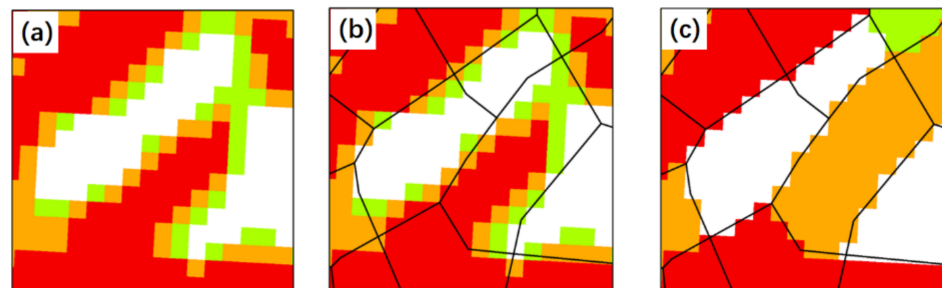


Figure 2. Schematic diagram of calculation method: (a) The transient rainfall infiltration and grid-based regional slope-stability model (TRIGRS) calculated safety factor diagram; (b) the boundary of the landslide is contrasted by the slope-units; (c) the results of the treatment using the slope-units.

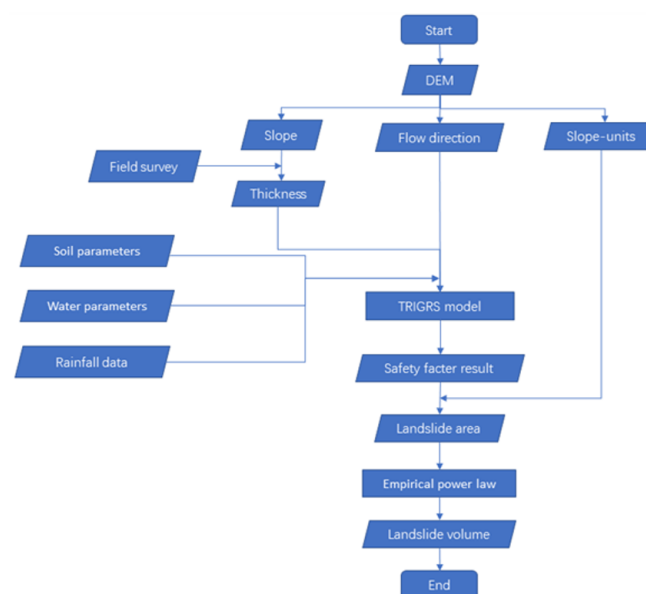


Figure 3. The workflow of this study.

3. Study Area and Data

3.1. Study Area

The Longxi River small watershed located in Wenchuan Earthquake Zone. It is part of the Minjiang River system and at the border of Wenchuan. The basin is located in the

subtropical humid monsoon climate region of the Sichuan Basin (Figure 4). The annual average rainfall is 1168.8 mm [35]. The annual monthly rainfall is unevenly distributed. The rainfall from May to September accounts for 80% of annual accumulated rainfall or more. The occurrence of geological disasters is often affected by the rainfall process. Due to the complex geological structure in Longxi River, the period from May to September is also the high occurrence period of geological disasters.

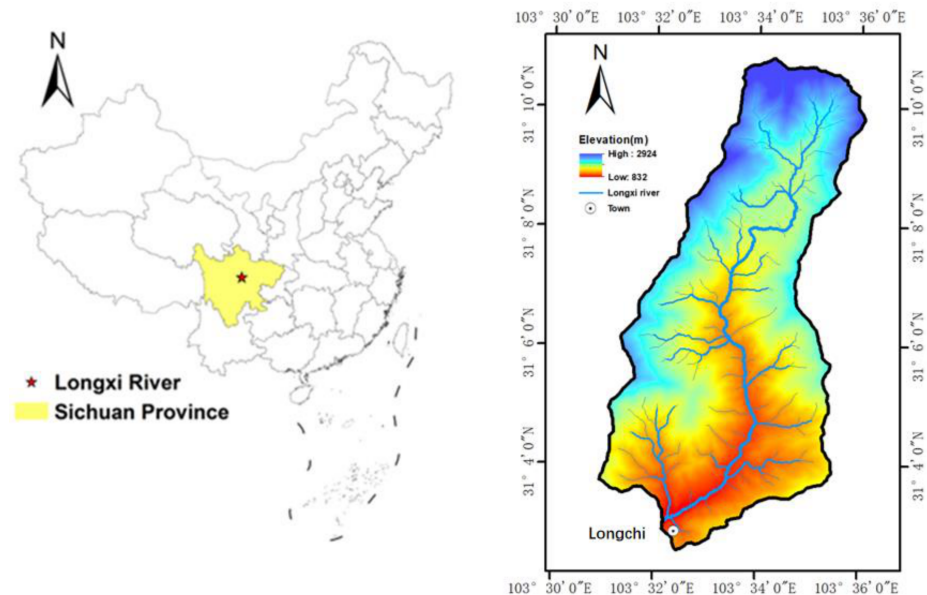


Figure 4. Geographic location and DEM of the Longxi River.

3.2. Rainfall Data

After the Wenchuan earthquake, heavy rainfall triggered a mudslide in Longchi on 13 August 2010. There were persistent thundershowers from 4 August to 12 August in the year. The average daily rainfall reached 28.7 mm. Starting from 3:30 in the afternoon, the rainfall reached 150 mm within three hours. The event caused a surge in geological hazards (Figure 5).

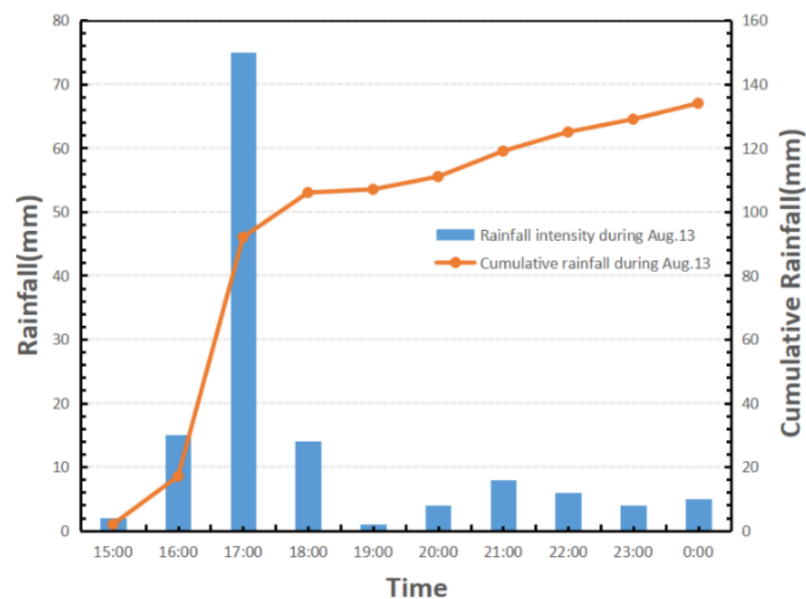


Figure 5. Rainfall data on 13 August 2010.

3.3. Field Survey

To obtain the change of soil moisture content in the Longxi River basin shown in Figure 6, we conducted five field surveys on 23 July, 7 September, 23 November 2019, and 11 January, 11 April 2020, respectively. The Maliu gully, a typical mountain flood gully, was selected for analysis of the variation of soil moisture. The antecedent precipitation in each survey is different. On 11 April 2020, the antecedent precipitation reached 19.8 mm in Longchi town, which is the maximum value of the five surveys. We selected six measurement positions along the gully in Figure 7. We selected three points on the slope for measurement in Figure 8, with an interval of 30 cm between each point. The average value of the three measurement values is taken as the value of the measurement point presented in Figure 9.

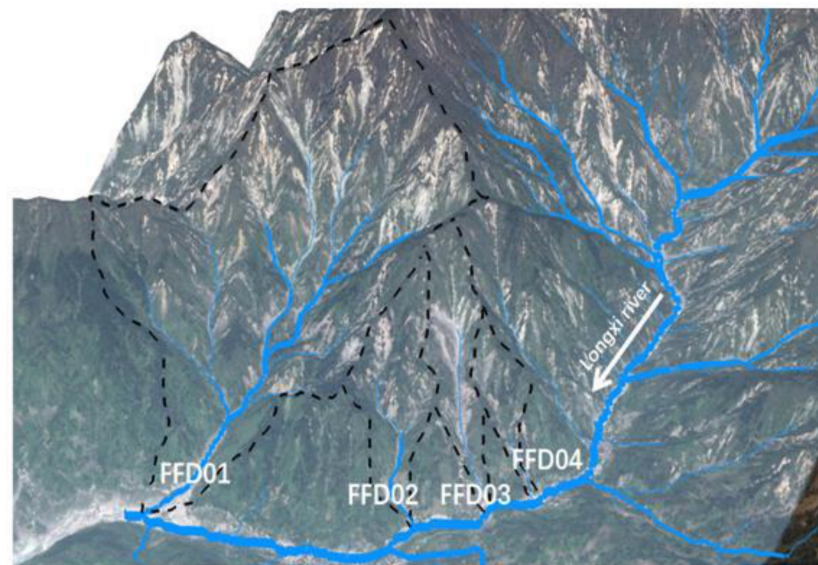


Figure 6. The location map of longxi river. (FFD01-Bayi gully, FFD02-Maliu gully, FFD03-Huangyang gully, FFD04-Shuida gully).

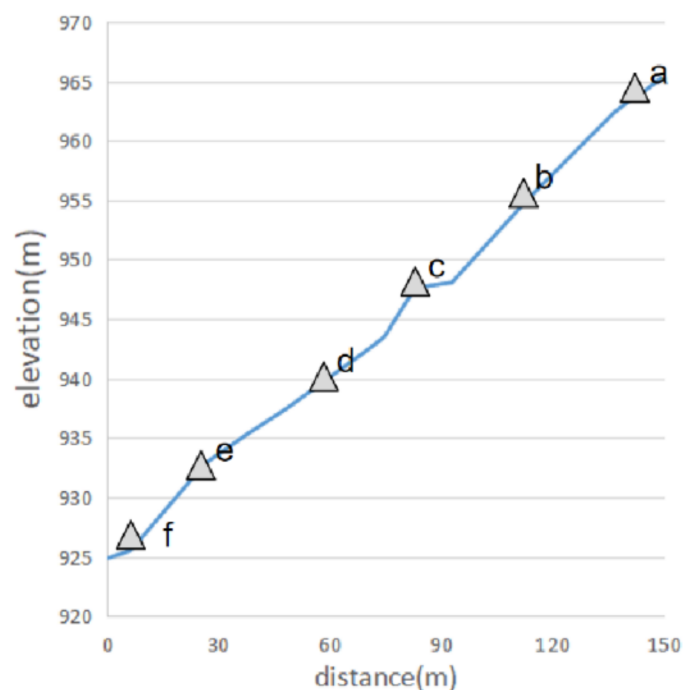


Figure 7. Elevation of measuring position in FFD02 (Maliu gully).

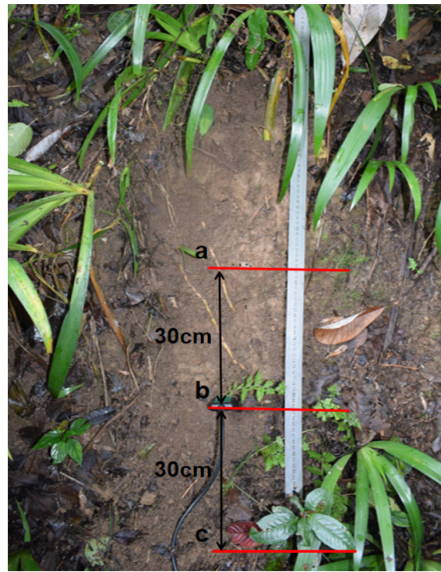


Figure 8. Soil moisture measurement in Longxi River Basin.

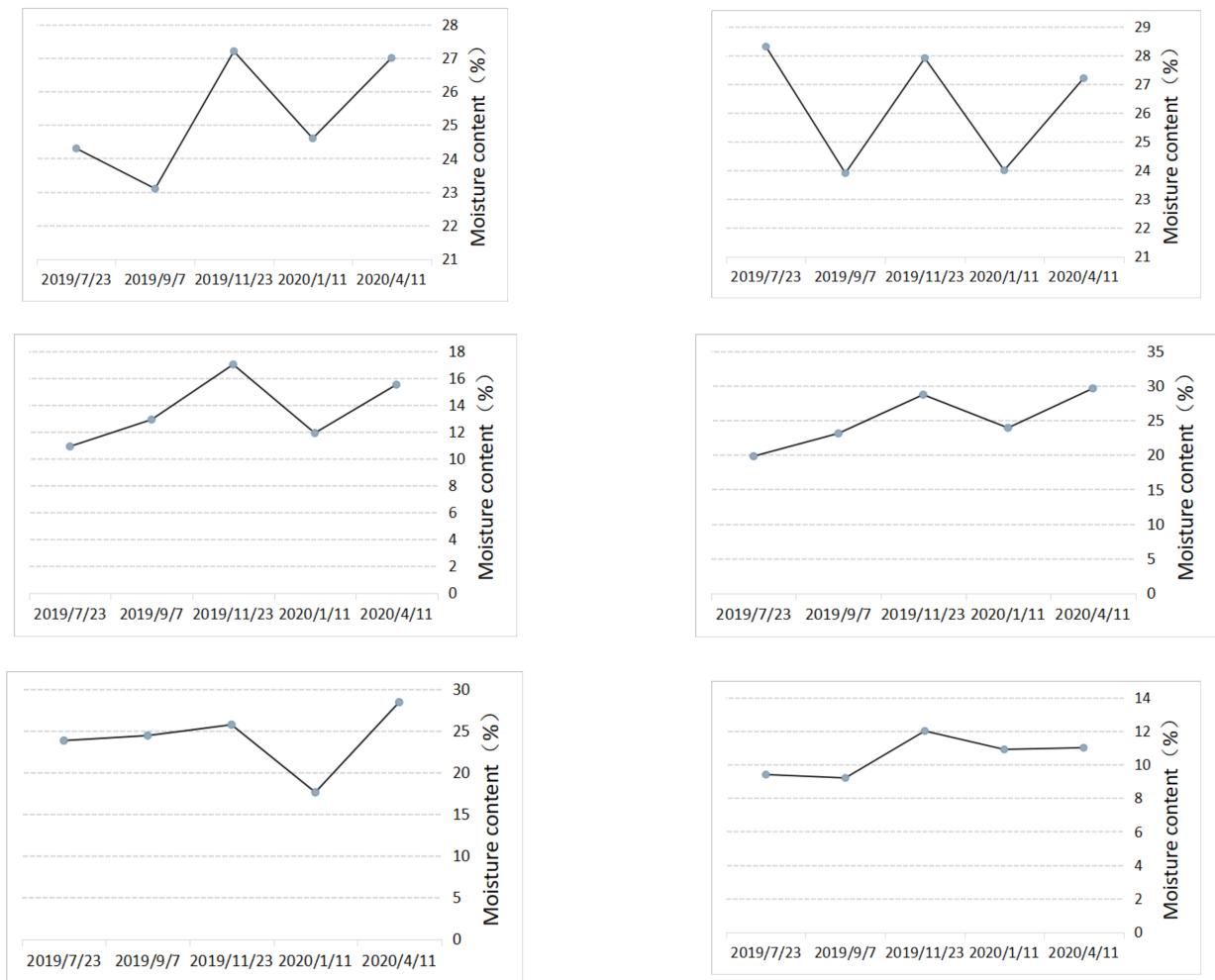


Figure 9. The water content of each measuring position.

3.4. Soil Parameters

In order to understand the influence of moisture content on soil mechanical parameters, Wang et al. conducted 60 triaxial experiments on the sandy loam [36]. The curve of internal friction angle and cohesion of moisture content shows cubic function relation.

$$C = 0.0096\omega^3 - 0.7593\omega^2 + 17.591\omega - 88.58 \quad (6)$$

$$C = -0.0014\omega^3 - 0.1098\omega^2 + 3.285\omega - 54.08 \quad (7)$$

The field survey shows that the soil moisture content in the Longxi River basin is about 23% in the rainy season under the condition of no significant early rainfall. Under the influence of previous rainfall, the maximum average soil moisture content reached 29%. This simulation was based on Wang's experimental results, and numerical simulation of the Longxi River basin was carried out with corresponding soil mechanical parameters at 29% (Table 1).

Table 1. Input soil parameters used in the application.

Soil cohesion c (kPa)	17.12
Soil friction angle ϕ ($^\circ$)	17.01
Soil unit weight γ (kN/m ³)	19.00

3.5. Hydraulic Parameters

Rawls et al. used multiple linear regression to estimate BC parameters from a large database of approximately 2540 soil layers [37,38]. Carsel and Parrish statistically processed the results to obtain the probability density function of VG parameters [39]. The water Flow parameter module of Hydrus 1D summarizes the results and obtains soil mechanical parameters of 12 soil types. Combined with the local soil type, the specific parameters are in the table below (Table 2).

Table 2. Input hydraulic parameters used in the application.

Residual soil water content θ_s	0.067
Saturated soil water content θ_r	0.45
Parameter α in the soil water retention function	0.02
Saturated hydrological conductivity K_S (m/s)	1.25×10^{-6}
Background infiltration rate I_{ZLT} (m/s)	1.25×10^{-8}

3.6. Soil Thickness

Soil thickness is the deepest possible failure surface of a landslide. Due to the lack of local data, the empirical function associated with the slope defined by Saulnier et al. was used to estimate the simulated soil thickness [40].

$$D_{Iz} = Z_{\max} \left[1 - \frac{\tan \delta - \tan \delta_{\min}}{\tan \delta_{\max} - \tan \delta_{\min}} \left(1 - \frac{Z_{\min}}{Z_{\max}} \right) \right] \quad (8)$$

Z_{\max} and Z_{\min} are the maximum and minimum values of soil thickness. δ_{\min} and δ_{\max} are the maximum and minimum values of the slope. According to the field investigation, Z_{\min} is set at 4 m and Z_{\max} at 0.4 m. The water table is considered to be the same as the soil thickness, as simulated by many other authors using TRIGRS [14,15,41] (Figures 10 and 11).

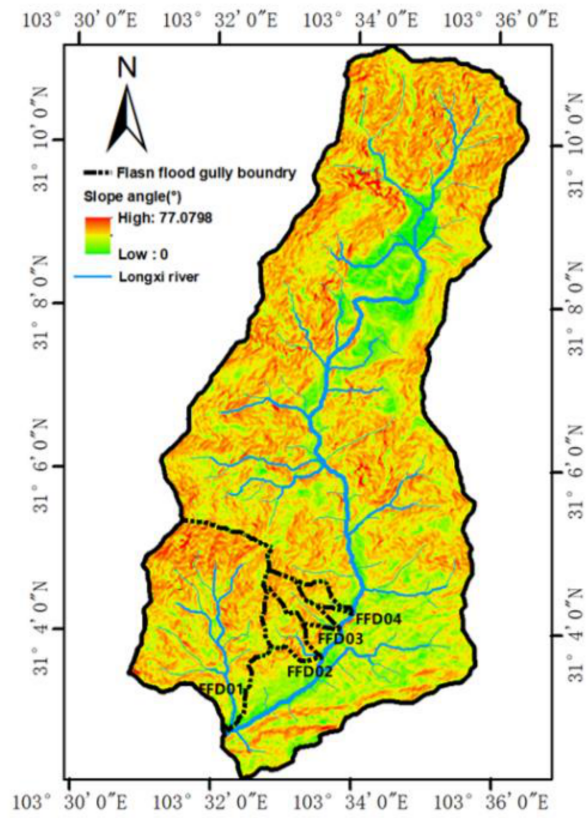


Figure 10. The slope figure of the Longxi River basin.

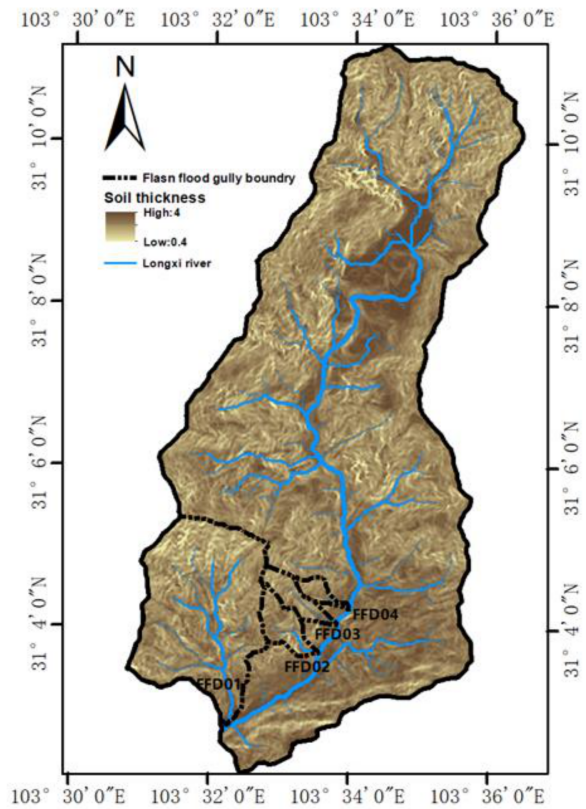


Figure 11. The soil thickness figure of the Longxi River basin.

4. Results

4.1. Estimated Area and Volume of Landslides

Since the four gullies are close together and the underlying surface conditions are similar, we applied the survey data to the other three gullies. Through the method, we get the safety factor distribution map of the basin. We divided the risk of the area into four levels based on the F_s value (Table 3). The resulting hazard distribution is shown in Figure 12.

Table 3. Hazard classification.

Rank	Rank of Index	Rank of Hazard
1	$0.8 < F_s \leq 0.9$	High
2	$0.9 < F_s \leq 0.95$	Moderate
3	$0.95 < F_s \leq 1$	Low
4	$1 < F_s \leq 10$	Safe

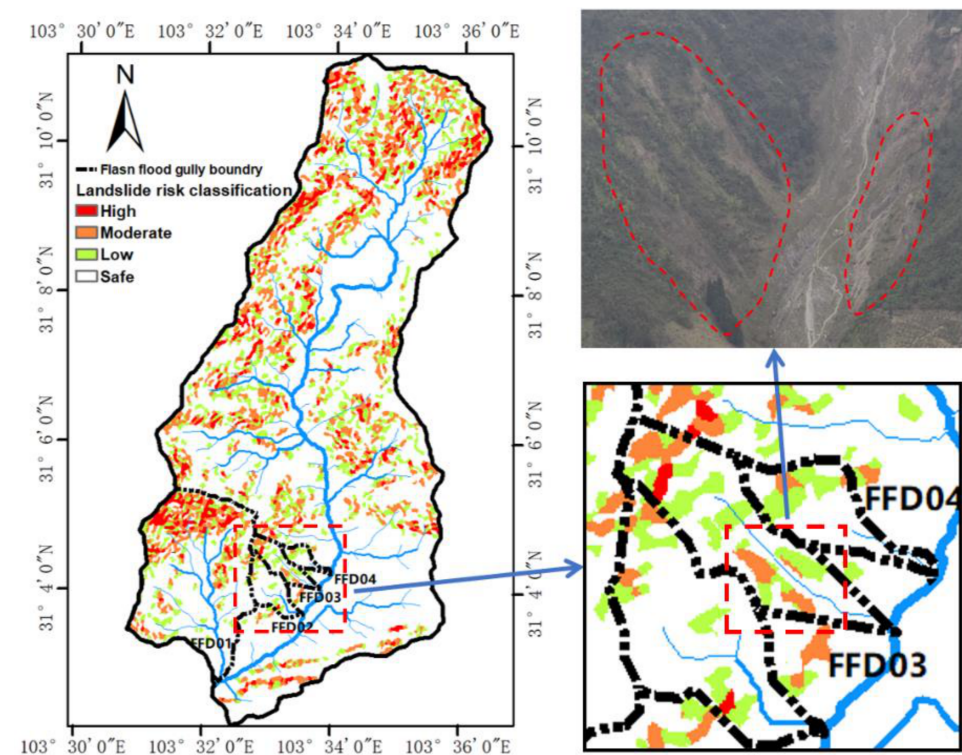


Figure 12. Rainfall data on 13 August 2010.

To verify the feasibility of the method, four typical gullies in the basin are selected. The volume of these gullies can be obtained from the post-disaster survey report [35]. We use the formula to calculate the volume of each landslide in the gully and get the potential volume of the landslide of each channel after segmentation and calculation (Table 4). On the whole, the values of LASU and LARSI are close. LASU in some valleys is slightly larger than LARSI. When a slope-unit is generally at risk, the slope-units partitioning method will define the safe grid-cells in the slope-unit as dangerous areas. This identification of the risk area makes the result higher than the actual interpretation result of satellite images. Except for Huangyang gully (FFD03), the estimated volume results of the remaining three gullies have similar situations. Through field investigation, it is found that the regional distribution of Huangyang gully landslide accords with the calculated results. The main reason for this situation is that there is a large number of loose deposits in the Huangyang gully, and TRIGRS cannot calculate this part of the volume, resulting in a large deviation between the calculated results and the actual survey data.

Table 4. Statistics of landslide area by interpretation satellite images (LAISI) (m^2), landslide area by slope-units (LASU) (m^2), landslide volume by post-disaster investigation (LVDI) (m^3), landslide volume by slope-units (LVSU) (m^3).

Number	Gully Name	LAISI	LASU	LVDI	LVSU
FFD1	Bayi	2,278,300	2,680,000	8,589,400	8,782,030
FFD2	Maliu	166,000	197,356	594,800	633,567
FFD3	Huangyang	250,000	259,531	1,435,000	934,884
FFD4	Shuida	72,800	81,250	212,100	261,470

4.2. Slope Distribution

To better understand the impact of slope on landslides in this area, we calculated the slope distribution of the landslide surface in the basin. According to the results, landslides are mainly distributed in slopes with a slope angle of $25\text{--}55^\circ$, and the average slope angle is about 40° (Figure 13).

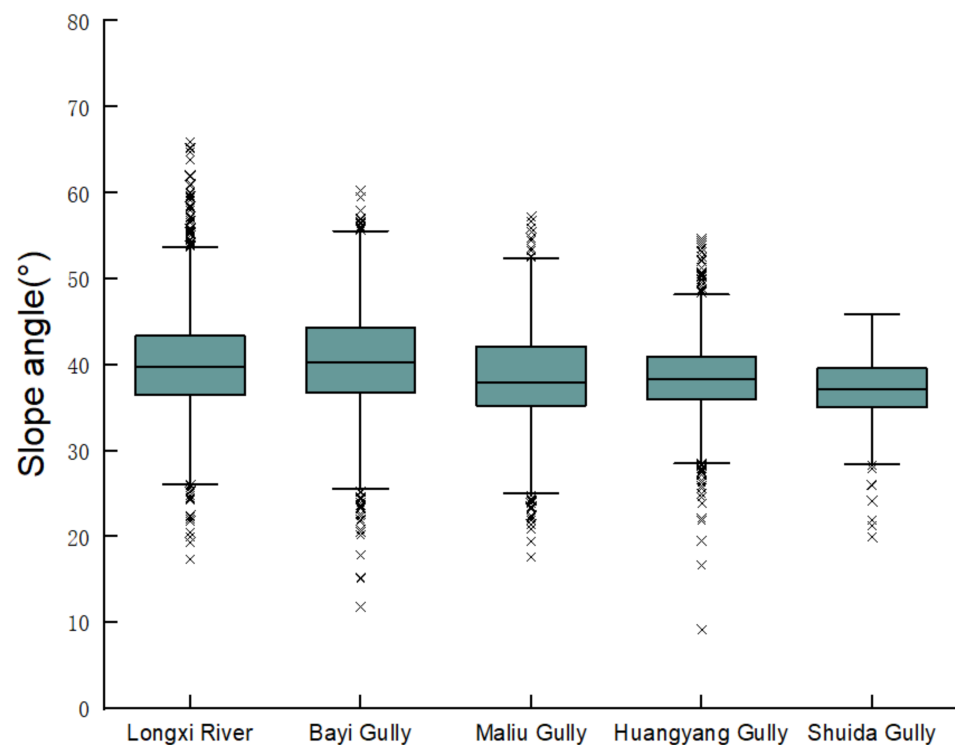


Figure 13. Distribution map of landslide slope angle.

Statistics show that there are a lot of steep slopes in the basin. The slope angle of the Longxi River basin is concentrated between 25° and 55° . The slope angle of $30\text{--}50^\circ$ accounts for 52.1% of the total area. The landslide risk area has a slope of 92.3% between $30\text{--}50^\circ$. The slope angle distribution of the four channels is slightly different, among which the $30\text{--}50^\circ$ slopes of the Bayi gully and Huangyang gully account for more than 60% of the basin. The $30\text{--}50^\circ$ slope of the Maliu gully and Shuida gully accounts for about 50% of the basin. It is found that the landslides in the Bayi gully and Huangyang gully are $1,021,000 m^3$ and $1,363,000 m^3$ per square kilometer. The average volume of the Maliu gully and Shuida gully landslides is smaller, being $736,300 m^3$ and $814,300 m^3$, respectively.

4.3. Variation Law of Soil Moisture

It was found that among the six positions in the Maliu gully, the soil sand content of the measuring point (c) in the middle of the gully and the measuring point (f) at the bottom of the gully increased significantly, which resulted in a significant drop in the corresponding

soil moisture content in Figure 9. Generally speaking, the annual soil moisture content is kept at about 23%, and the water content of some points is enriched. The soil moisture content in summer is greater than that in other seasons. When rainfall occurs, soil moisture content increases rapidly. The soil along the gully is unsaturated for a long time in a year.

To explore the influence of the water content change of the watershed on the regional stability, considering the above analysis of soil content in the field investigation, four additional groups with different water contents of 27%, 28%, 30%, and 31% were selected for simulation. The results show that there is no disaster area in the basin when the soil moisture is 27%. When the water content reaches 28%, a large area of disaster occurs in the basin. With the increase of the moisture content, the area of the danger zone continues to expand, and the level of danger increases accordingly (Figures 14 and 15).

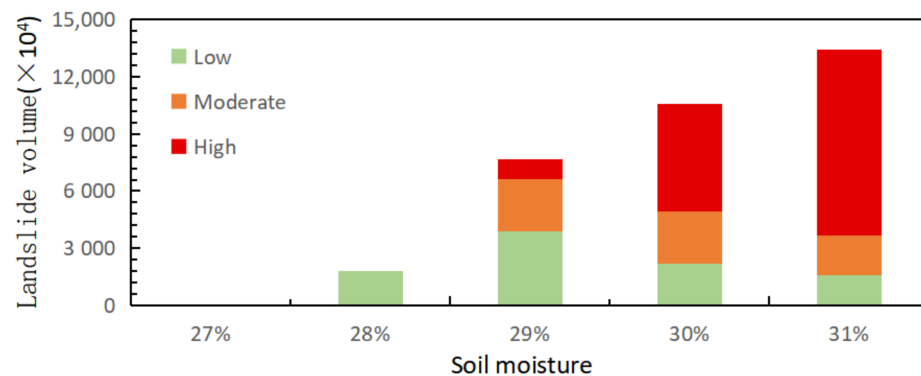


Figure 14. Landslide volume with different soil water content.

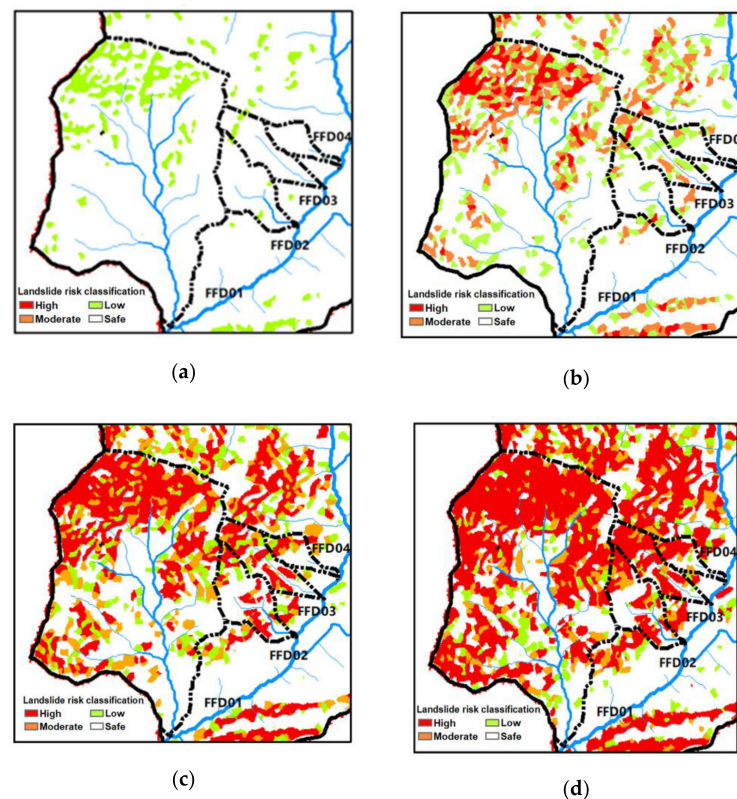


Figure 15. Distribution map of safety factor under different soil moisture content (a) 28%; (b) 29%; (c) 30%; (d) 31%.

When the water content is 28%, there are only low-risk areas in the entire basin. The danger zone is mainly distributed in the upper reaches of the gully, where the slope angle

is large. With the continuous increase of water content, low-risk areas have gradually transformed into high-risk areas, while new risk areas have also grown. The dangerous zone is generated from the upper valley, gradually to both sides of the channel development. When the water content reaches 31%, a large area of disaster has already occurred in the basin.

5. Discussion

To judge whether the results obtained by the proposed calculation procedure are consistent with the actual results, the calculated results for part of mountain flood gullies with large landslide areas are selected for comparison with the results obtained by Chang et al. through the satellite images [19]. It is found that by extracting the results from the slope-units, there are some errors between the area obtained from some ditches and the actual satellite images, but the overall relative error is relatively small, which is more consistent with the reality.

The volume of flash flood gullies was also compared with the survey report of landslide source volume after a flood disaster [35]. The results show that the proposed method is reliable in estimating the provenance volume. The error of the other three gullies except the Huangyang gully is small. As for the error source of the Huangyang gully, the field investigation suggests that the main reason may be because of a large number of loose accumulation bodies in the channel. TRIGRS cannot be used to make statistics on this part, which leads to a small estimate of the landslide volume in the basin.

After extracting the landslide slope angle for the landslide area, it is found that more than 90% of the landslides have a slope angle between 30° and 50° , indicating an average gradient of around 40° for the landslides. To explore the impact of the basin slope on the landslide, the slopes of the four gullies were compared with the landslide volume per square kilometer. The results showed that the 30° – 50° slope of the Maliu gully and Shuida gully accounted for about 50% of the total slope, and the sediment yields of the basin were $73.6 \times 10^4 \text{ m}^3/\text{km}^2$ and $81.4 \times 10^4 \text{ m}^3/\text{km}^2$, respectively, indicating the average potential square capacity of the basin. The ratios of 30° – 50° slopes of the Bayi gully and Huangyang gully are both above 60%, and the potential square quantities of the two channels are $102.1 \times 10^4 \text{ m}^3/\text{km}^2$ and $136.3 \times 10^4 \text{ m}^3/\text{km}^2$, respectively. It can be seen that there is a great correlation between slope distribution and landslide volume in the gully. The slope of 30° – 50° is the main area where landslides occur, and the proportion of this area in the total drainage basin also affects the volume of landslides. When the slope is more distributed around 40° , the landslide volume per square kilometer will be larger in the basin.

As the moisture content changes, it affects the changes in soil parameters. The watershed will have a sudden change when the water content reaches 28%, resulting in a large number of landslide areas. With the continuous increase of water content, the area of landslides in the basin and the level of danger continue to increase. The landslide first occurred far upstream of the gully, away from the channel, where it usually does not enter and cause changes in sediment concentration. With the increase of the water content, the distribution of landslides gradually draws closer to the river. It is known from field measurement that the moisture content will change greatly with the previous rainfall. The maximum moisture content in some areas can reach 29%. However, the average water content of the whole basin is usually around 26%, which means that the basin is in a safe state. The “8.13” the disaster caused a large number of landslides and debris flows throughout the river basin. There were continuous thundershowers in the nine days before the “8.13” disaster. One of the key reasons for the “8.13” disaster was that the water content increased significantly due to previous rainfall. This shows that the change of local soil moisture content before the occurrence of mountain torrents significantly affects the occurrence of landslides. In future early warning of mountain torrent disasters, the monitoring of water content can increase the accuracy of early warning.

To explore how the moisture content affects the final result, we conducted a sensitivity analysis of the internal friction angle and cohesion. We selected the range of internal friction angle and cohesion under the condition of 27–31% moisture content as the scope of this analysis (Figure 16). The results showed that the area and volume of the landslide decreased significantly with the increase of cohesion. When the cohesion reaches 22 kPa, there is no landslide in the basin. The area and volume of the landslide are relatively weakly sensitive to the angle of internal friction. Based on the above results, we believe that the moisture content mainly affects the calculation results of the model for landslides by affecting the cohesion of the soil.

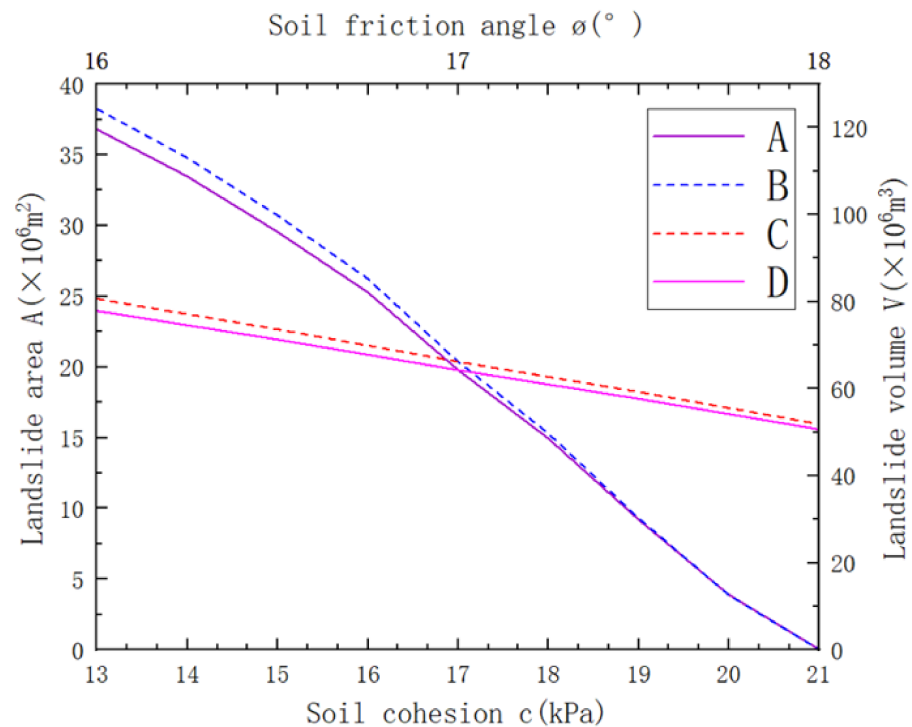


Figure 16. Sensitivity analysis results on friction angle and cohesion; (A) relationship curve between cohesion and landslide area; (B) relationship curve between cohesion and landslide volume; (C) relationship curve between friction angle and landslide volume; (D) relationship curve between friction angle and landslide area.

When an empirical power law formula is applied to the interpretation of satellite images, landslide volume is often overestimated due to the existence of landslide clusters [42]. Marc et al. proposed an algorithm to distinguish landslide clusters based on a digital elevation model (DEM) and a raster file of polygon shapes [43]. Fan et al. proposed to cut the landslide clusters through the flow direction to reduce the impact of the landslide clusters [44]. Calculating landslide volume through TRIGRS is also affected by landslide clusters. In the slope-units partitioning method, the boundary of slope-units is used to cut the landslide risk map, thereby reducing the impact of the landslide cluster. A dangerous slope-unit is considered an independent landslide.

From the results, the estimated volume is somewhat different from the actual surveyed volume. DEM data of 12.5 m \times 12.5 m specification is of relatively low accuracy, which leads to the inaccuracy of calculation results. Due to the lack of data in this simulation, differences in soil and space conditions, such as vegetation, were not taken into account, which also leads to inaccurate calculation results. In addition, a large number of loose deposits in the channel are also the material source of mountain torrent disasters. This method cannot estimate the volume of this part, resulting in a small estimation result of some gullies.

6. Conclusions

In this paper, we propose a method for extracting and optimizing the calculation results of the safety factor of TRIGRS by using the slope-units, and estimating the potential landslide volume in the basin by combining the appropriate empirical power-law formula. To verify the reliability of the method, four local basins in the Longxi River basin were processed and calculated. The area and volume obtained were compared with the interpretation of satellite images and field survey results respectively. The main results are summarized as follows:

The method presented in this paper is reliable for landslide volume estimation in a mountainous watershed, which can be used to study the impact of sediment transport on mountain torrent disasters in the basin. The slope-units proved to be an effective parameter for cutting landslide clusters. The volume of the slope unit is in good agreement with the results of the disaster investigation.

Statistics show that the landslide surface in the Longxi River basin is concentrated at the slope angle of 30–50°. It is proved that there is a high correlation between landslide volume and slope angle in the basin. The slope distribution can be used as a reference factor when considering the influence of sediment recharge in the future.

The previous rainfall amount will significantly affect the soil moisture content, thus affecting the overall stability of the landslide in the basin. When the mountain flood disaster is analyzed, the previous conditions should be analyzed concretely.

Author Contributions: T.S. proposed the method; T.S. organized and wrote this paper. Z.D. and Z.X. made the field investigation and analyzed the data. X.W. revised the manuscript. All authors have read and agreed to the published version of the manuscript.

Funding: This research is supported by the National Key R&D Program of China (2017YFC1502504), the National Natural Science Foundation of China (51639007 and 41771543) and the Open Foundation projects (SKHL1913, SKHL1804), State Key Laboratory of Hydraulics and Mountain River Engineering, Sichuan University. Thanks to two anonymous reviewers and editors for their useful and careful critiques for improving this research.

Informed Consent Statement: Not applicable.

Data Availability Statement: The data presented in this study are available on request from the corresponding author.

Conflicts of Interest: The authors declare no conflict of interest.

References

1. Duan, W.L.; He, B.; Nover, D.; Fan, J.L.; Yang, G.S.; Chen, W.; Meng, H.F.; Liu, C.M. Floods and associated socioeconomic damages in China over the last century. *Nat. Hazards* **2016**, *82*, 401–413. [[CrossRef](#)]
2. Tu, H.W.; Wang, X.K.; Zhang, W.S.; Peng, H.; Ke, Q.; Chen, X.M. Flash Flood Early Warning Coupled with Hydrological Simulation and the Rising Rate of the Flood Stage in a Mountainous Small Watershed in Sichuan Province, China. *Water* **2020**, *12*, 255. [[CrossRef](#)]
3. Chen, X.Z.; Cui, Y.F. The formation of the Wulipo landslide and the resulting debris flow in Dujiangyan City, China. *J. Mt. Sci.* **2017**, *14*, 1100–1112. [[CrossRef](#)]
4. Wang, J.; Jin, Z.D.; Hilton, R.G.; Zhang, F.; Densmore, A.L.; Li, G.; West, A.J. Controls on fluvial evacuation of sediment from earthquake-triggered landslides. *Geology* **2015**, *43*, 115–118. [[CrossRef](#)]
5. Parker, R.N.; Densmore, A.L.; Rosser, N.J.; de Michele, M.; Li, Y.; Huang, R.Q.; Whadcoat, S.; Petley, D.N. Mass wasting triggered by the 2008 Wenchuan earthquake is greater than orogenic growth. *Nat. Geosci.* **2011**, *4*, 449–452. [[CrossRef](#)]
6. Tang, Y.X.; Zhang, Z.J.; Wang, C.; Zhang, H.; Wu, F.; Zhang, B.; Liu, M. The deformation analysis of Wenjiagou giant landslide by the distributed scatterer interferometry technique. *Landslides* **2018**, *15*, 347–357. [[CrossRef](#)]
7. Zhou, J.W.; Cui, P.; Yang, X.G.; Su, Z.M.; Guo, X.J. Debris flows introduced in landslide deposits under rainfall conditions: The case of Wenjiagou gully. *J. Mt. Sci.* **2013**, *10*, 249–260. [[CrossRef](#)]
8. Ran, Q.H.; Qian, Q.; Li, W.; Fu, X.D.; Yu, X.; Xu, Y.P. Impact of earthquake-induced-landslides on hydrologic response of a steep mountainous catchment: A case study of the Wenchuan earthquake zone. *J. Zhejiang Univ. Sci. A* **2015**, *16*, 131–142. [[CrossRef](#)]
9. Dietrich, W.E.; Wilson, C.J.; Montgomery, D.R.; McKean, J. Analysis of erosion thresholds, channel networks, and landscape morphology using a digital terrain model. *J. Geol.* **1993**, *101*, 259–278. [[CrossRef](#)]

10. Dietrich, W.E.; Reiss, R.; Hsu, M.L.; Montgomery, D.R. A process-based model for colluvial soil depth and shallow landsliding using digital elevation data. *Hydrol. Process.* **1995**, *9*, 383–400. [[CrossRef](#)]
11. Montgomery, D.R.; Dietrich, W.E. A physically-based model for the topographic control on shallow landsliding. *Water Resour. Res.* **1994**, *30*, 1153–1171. [[CrossRef](#)]
12. Baum, R.L.; Savage, W.Z.; Godt, J.W.J.O.-F.R. *TRIGRS-A Fortran Program for Transient Rainfall Infiltration and Grid-Based Regional Slope-Stability Analysis*; US Geological Survey Open-File Report; US Geological Survey: Reston, VA, USA, 2002.
13. Baum, R.L.; Savage, W.Z.; Godt, J.W.J.O.-F.R. *TRIGRS—A Fortran Program for Transient Rainfall Infiltration and Grid-Based Regional Slope-Stability Analysis, Version 2.0*; US Geological Survey Open-File Report; US Geological Survey: Reston, VA, USA, 2008.
14. Tang, Y.; Yin, K.-L.; Liu, L.; Zhang, L.; Fu, X.-L. Dynamic assessment of rainfall-induced shallow landslide hazard. *J. Mt. Sci.* **2017**, *14*, 1292–1302. [[CrossRef](#)]
15. Marin, R.J.; Velasquez, M.F. Influence of hydraulic properties on physically modelling slope stability and the definition of rainfall thresholds for shallow landslides. *Geomorphology* **2020**, *351*, 14. [[CrossRef](#)]
16. Chen, Y.-L.; Chen, D.-H.; Li, Z.-C.; Huang, J.-B. Preliminary studies on the dynamic prediction method of rainfall-triggered landslide. *J. Mt. Sci.* **2016**, *13*, 1735–1745. [[CrossRef](#)]
17. Tang, C.X.; Tanyas, H.; van Westen, C.J.; Tang, C.; Fan, X.M.; Jetten, V.G. Analysing post-earthquake mass movement volume dynamics with multi-source DEMs. *Eng. Geol.* **2019**, *248*, 89–101. [[CrossRef](#)]
18. Fan, J.R.; Zhang, X.Y.; Su, F.H.; Ge, Y.G.; Tarolli, P.; Yang, Z.Y.; Zeng, C.; Zeng, Z. Geometrical feature analysis and disaster assessment of the Xinmo landslide based on remote sensing data. *J. Mt. Sci.* **2017**, *14*, 1677–1688. [[CrossRef](#)]
19. Chang, M.; Tang, C.; Ni, H.Y.; Qu, Y.P. Evolution process of sediment supply for debris flow occurrence in the Longchi area of Dujiangyan City after the Wenchuan earthquake. *Landslides* **2015**, *12*, 611–623. [[CrossRef](#)]
20. Tang, C.; Zhu, J.; Chang, M.; Ding, J.; Qi, X. An empirical-statistical model for predicting debris-flow runout zones in the Wenchuan earthquake area. *Quat. Int.* **2012**, *250*, 63–73. [[CrossRef](#)]
21. Chiu, Y.J.; Lee, H.Y.; Wang, T.L.; Yu, J.Y.; Lin, Y.T.; Yuan, Y.P. Modeling Sediment Yields and Stream Stability Due to Sediment-Related Disaster in Shihmen Reservoir Watershed in Taiwan. *Water* **2019**, *11*, 332. [[CrossRef](#)]
22. Guzzetti, F.; Ardizzone, F.; Cardinali, M.; Rossi, M.; Valigi, D. Landslide volumes and landslide mobilization rates in Umbria, central Italy. *Earth Planet. Sci. Lett.* **2009**, *279*, 222–229. [[CrossRef](#)]
23. Larsen, I.J.; Montgomery, D.R.; Korup, O. Landslide erosion controlled by hillslope material. *Nat. Geosci.* **2010**, *3*, 247–251. [[CrossRef](#)]
24. Guzzetti, F.; Carrara, A.; Cardinali, M.; Reichenbach, P. Landslide hazard evaluation: A review of current techniques and their application in a multi-scale study, Central Italy. *Geomorphology* **1999**, *31*, 181–216. [[CrossRef](#)]
25. Wang, K.; Zhang, S.J.; DelgadoTellez, R.; Wei, F.Q. A new slope unit extraction method for regional landslide analysis based on morphological image analysis. *Bull. Eng. Geol. Environ.* **2019**, *78*, 4139–4151. [[CrossRef](#)]
26. Romstad, B.; Etzelmuller, B. Mean-curvature watersheds: A simple method for segmentation of a digital elevation model into terrain units. *Geomorphology* **2012**, *139*, 293–302. [[CrossRef](#)]
27. Yan, G.; Liang, S.Y.; Zhao, H.L. An Approach to Improving Slope Unit Division Using GIS Technique. *Sci. Geogr. Sin.* **2017**, *11*, 1764–1770.
28. Alvioli, M.; Marchesini, I.; Reichenbach, P.; Rossi, M.; Ardizzone, F.; Fiorucci, F.; Guzzetti, F. Automatic delineation of geomorphological slope units with r.slopeunits v1.0 and their optimization for landslide susceptibility modeling. *Geosci. Model Dev.* **2016**, *9*, 3975–3991. [[CrossRef](#)]
29. Alvioli, M.; Guzzetti, F.; Rossi, M. Scaling properties of rainfall induced landslides predicted by a physically based model. *Geomorphology* **2014**, *213*, 38–47. [[CrossRef](#)]
30. Wang, K.; Xu, H.; Zhang, S.J.; Wei, F.Q.; Xie, W.L. Identification and Extraction of Geomorphological Features of Landslides Using Slope Units for Landslide Analysis. *ISPRS Int. Geo-Inf.* **2020**, *9*, 274. [[CrossRef](#)]
31. Alvioli, M.; Baum, R.L. Parallelization of the TRIGRS model for rainfall-induced landslides using the message passing interface. *Environ. Model. Softw.* **2016**, *81*, 122–135. [[CrossRef](#)]
32. Srivastava, R.; Yeh, T.C.J. Analytical solutions for one-dimensional, transient infiltration toward the water-table in homogeneous and layered soils. *Water Resour. Res.* **1991**, *27*, 753–762. [[CrossRef](#)]
33. Iverson, R.M. Landslide triggering by rain infiltration. *Water Resour. Res.* **2000**, *36*, 1897–1910. [[CrossRef](#)]
34. Gardner, W.R. Some steady-state solutions of the unsaturated moisture flow equation with application to evaporation from a water table. *Soil sci.* **1958**, *85*, 228–232. [[CrossRef](#)]
35. Cheng, S. Vulnerability Assessment for Post-Earthquake Coincident Debris Flows in Longxihe River Basin, Dujiangyan City. Ph.D. Thesis, Chengdu University of Technology, Chengdu, China, 2015.
36. Wang, J.F.; Guo, L.F.; Du, C.X.; Zhu, X.X. Effect of Water Content and Dry Density on Shear Strength of Sandy Loam Soil. *Pearl River* **2019**, *40*, 19–22.
37. Rawls, W.J.J.A. Estimating soil water properties. *Trans. ASAE* **1982**, *25*, 1316–1320. [[CrossRef](#)]
38. Simunek, J.J.H.S. *The HYDRUS 1D Software Package for Simulating the One-Dimensional Movement of Water, Heat, and Multiple Solutes in Variably Saturated Porous Media*, version 3.0; HYDRUS Software Series 1; Department of Environmental Sciences, University of California Riverside: Riverside, CA, USA, 2005.

39. Carsel, R.F.; Parrish, R.S. Developing joint probability-distributions of soil-water retention characteristics. *Water Resour. Res.* **1988**, *24*, 755–769. [[CrossRef](#)]
40. Saulnier, G.M.; Beven, K.; Obed, C. Including spatially variable effective soil depths in TOPMODEL. *J. Hydrol.* **1997**, *202*, 158–172. [[CrossRef](#)]
41. Park, D.W.; Nikhil, N.V.; Lee, S.R. Landslide and debris flow susceptibility zonation using TRIGRS for the 2011 Seoul landslide event. *Nat. Hazards Earth Syst. Sci.* **2013**, *13*, 2833–2849. [[CrossRef](#)]
42. Li, G.; West, A.J.; Densmore, A.L.; Jin, Z.D.; Parker, R.N.; Hilton, R.G. Seismic mountain building: Landslides associated with the 2008 Wenchuan earthquake in the context of a generalized model for earthquake volume balance. *Geochem. Geophys. Geosyst.* **2014**, *15*, 833–844. [[CrossRef](#)]
43. Marc, O.; Hovius, N. Amalgamation in landslide maps: Effects and automatic detection. *Nat. Hazards Earth Syst. Sci.* **2015**, *15*, 723–733. [[CrossRef](#)]
44. Fan, R.L.; Zhang, L.M.; Shen, P. Evaluating volume of coseismic landslide clusters by flow direction-based partitioning. *Eng. Geol.* **2019**, *260*, 11. [[CrossRef](#)]